Supplementary Information for

Interaction Hot Spots for Phase Separation Revealed by NMR Studies of a CAPRIN1 Condensed Phase

Tae Hun Kim, Brandon J. Payliss, Michael L. Nosella, Ian T. W. Lee,
Yuki Toyama, Julie D. Forman-Kay* and Lewis E. Kay*

* Corresponding authors: Lewis E. Kay (kay@pound.med.utoronto.ca), Julie D. Forman-Kay (forman@sickkids.ca)

This PDF file includes:

Materials and Methods

Protein production

The C-terminal low complexity domain of CAPRIN1 (607-709) was expressed and purified as described in our previous studies (1, 2). Briefly, CAPRIN1 with an N-terminal His-SUMO tag was expressed in BL21 (DE3) *E. coli* cells. For preparing ^{12}C, ^{14}N, ^{1}H samples, the auto-induction medium, ZYM-5052, described previously (3), was used and IPTG induction was not

necessary. ^{13}C, ^{15}N, ^{1}H and ^{13}C, ^{14}N, ^{1}H samples were prepared by growing cell cultures in M9 minimal medium (6 g of Na_2HPO_4, 3 g of KH_2PO_4, 0.5 g of NaCl, 2 mM of $MgSO_4$, 100 μM of $CaCl_2$, 3 g of [U^{13}C]-glucose, 50 μg/mL of kanamycin, 10 mg of each of biotin and thiamine in 1 L of buffer, pH 7.4) with 1 g of either $^{15}NH_4Cl$ (^{15}N-labeled protein) or natural abundance NH_4Cl. ^{12}C, ^{15}N, ^{2}H samples were prepared using the same M9 minimal medium but with 3 g of [d7]-glucose, and 1 g of $^{15}NH_4Cl$ added to 1 L of 99% D_2O (Cambridge Isotope Laboratories). For isotope-labeled protein expression, cell cultures were induced with 0.5 mM IPTG at 25°C for 12-18 hours. After harvesting, the cell pellets were lysed by sonicating the cell suspension in lysis buffer (6 M guanidine hydrochloride (GuHCl), 25 mM Tris, 500 mM NaCl, 20 mM imidazole, 2 mM β-mercaptoethanol, pH 8.0) and centrifuged (23,000 g, 30 min, at 4°C). Subsequently, the supernatant was loaded onto a Ni-NTA column (GE Healthcare) pre-equilibrated with lysis buffer. The Ni-NTA column was washed with 10 column volumes of lysis buffer, followed by 3 column volumes of wash buffer (25 mM Tris, 500 mM NaCl, 20 mM imidazole, 2 mM β-mercaptoethanol, pH 8.0). The His-SUMO-CAPRIN1 bound to Ni-NTA resin was eluted with elution buffer (25 mM Tris, 500 mM NaCl, 300 mM imidazole, 2 mM β-mercaptoethanol, pH 8.0). After dialysis with His-ULP1 protease against cleavage buffer (25 mM Tris, 150 mM NaCl, 2 mM β-mercaptoethanol, pH 8.0), the solution was applied to Ni-NTA to separate CAPRIN1 from His-SUMO and His-ULP1 protease. CAPRIN1 was further purified by FPLC equipped with a Superdex 75 16/60 column equilibrated with gel filtration buffer (3 M GuHCl, 25 mM Tris, 500 mM NaCl, 2 mM β-mercaptoethanol, pH 8.0). Finally, the pure CAPRIN1 fraction was verified with SDS-PAGE and collected. CAPRIN1 mutant plasmids ($GYR_{(624-626)}$, $GYR_{(638-640)}$, $RDY_{(660-662)}$, $QSG_{(680-682)}$, $NTQ_{(704-706)}$ to ASA) were prepared by using the QuikChange mutagenesis strategy. For quantifying protein concentrations, predicted molar extinction

coefficients of 10,430 $M^{-1}cm^{-1}$ (Wildtype, $QSG_{(680-682)}$, $NTQ_{(704-706)}$ mutants) and 8,940 $M^{-1}cm^{-1}$ ($GYR_{(624-626)}$, $GYR_{(638-640)}$, $RDY_{(660-662)}$ mutants) were used. The mutant CAPRIN1 constructs were expressed and purified using the same procedures described above.

For fluorescence imaging of CAPRIN1, a mutant CAPRIN1 construct with an extra cysteine at the C-terminus was used to prepare Alexa647-labelled CAPRIN1 using maleimide conjugation chemistry. The purified CAPRIN1-Cys mutant dissolved in pre-reaction buffer (3 M GuHCl, 25 mM HEPES, 2 mM DTT at pH 7.0) was buffer-exchanged into maleimide conjugation buffer (3 M GuHCl, 25 mM HEPES at pH 7.0) using an FPLC setup equipped with a 5 mL HiTrap desalting column. Subsequently, Alexa647-maleimide (ThermoFisher Scientific) dissolved in DMF was added to the desalted protein fraction, generating a concentration of Alexa647-maleimide that is 5-10 times in excess of CAPRIN1-Cys. The conjugation reaction was carried at 4°C for 12-18 hours and quenched by adding 5 mM DTT. Alexa647-CAPRIN1 was purified chromatographically from unreacted Alexa647 fluorophores with a 5 mL HiTrap desalting column followed by a Superdex 75 16/60 column. Fluorescein (FITC)-labelled CAPRIN1 was prepared with FITC-5-maleimide (ThermoFisher Scientific) using the same protocol.

Turbidity assays

Purified CAPRIN1 samples were diluted to a protein concentration of 300 μM with 25 mM MES, pH 5.5 containing varying concentrations of NaCl ranging from 0 to 2000 mM. After rigorous mixing, 5 μL samples were loaded into a μCuvette G1.0 (Eppendorf). OD600 measurements were recorded three times using a BioPhotometer D30 (Eppendorf).

Fluorescence imaging

CAPRIN1 samples used for fluorescence imaging contained 5-10% of Alexa647/FITC-labelled CAPRIN1. CAPRIN1 and ATP-Mg were prepared in imaging buffer (25 mM HEPES, 2 mM DTT, pH 7.4). CAPRIN1 droplets were generated by adding ATP-Mg pre-mixed with 2% TNP-ATP (ThermoFisher Scientific) to CAPRIN1 solutions. After rigorous mixing, protein solutions with varying concentrations of ATP-Mg were placed onto 96 well glass-bottom plates (Eppendorf). To allow droplets to sediment to the bottom of the plate, there was a 5 min waiting period prior to imaging. All images were taken using a Leica DMi8 confocal microscope equipped with a Hamamatsu C9100-13 EM-CCD camera. Fluorescence images of Alexa647 and TNP-ATP/FITC were acquired using lasers at 637 nm (50 mW) and 491 nm (50 mW) wavelengths, respectively. All images were analyzed with Volocity (PerkinElmer) and ImageJ (NIH).

Construction of phase diagrams

Purified CAPRIN1 was prepared in mixed-state NMR buffer (25 mM MES at pH 5.5). To induce phase separation, a NaCl stock solution (25 mM MES, 2 M NaCl at pH 5.5) was added to purified CAPRIN1 in Eppendorf tubes to make a range of final NaCl concentrations (*i.e*. 200, 300, 400, 600 mM, Fig. 3*A*). Three protein samples were prepared to obtain triplicate measurements. After rigorous vortexing, the phase-separated samples were incubated at the desired temperatures using a thermocycler with a heated lid (95°C). At least 1 hour was required to allow droplets to form a large condensed phase at the bottom of the tubes. For temperatures below 15°C, the waiting period was extended to 2 hours. Once a large condensed phase was formed, a positive displacement pipettor and tips (Eppendorf) were used to pipette 2 and 10 µL

of condensed and dilute phases, respectively. Notably, using a positive displacement pipettor and tips was important for accurate pipetting of the viscous condensed phase. After diluting the condensed- (500 times) and dilute- (10-40 times) phase samples into a denaturing buffer (6 M GuHCl, 25 mM $NaPO_4$ at pH 7.4), the A280 value was measured using a BioPhotometer D30 (Eppendorf). Protein concentrations were determined using a predicted molar extinction coefficient of 10,430 $M^{-1}cm^{-1}$. Errors were generated by taking standard deviations of the triplicate measurements. The phase diagram was fitted to simple Flory-Huggins theory, as described in our previous study (4).

Preparation of GlcNAc-CAPRIN1

The pET24b vector containing the open reading frame for full-length, *H. sapiens O*-GlcNAc transferase (OGT; nucleocytoplasmic variant, 110 kDa) was a kind gift from Dr. Suzanne Walker. OGT was expressed and purified from *E. coli* BL21 (DE3) RIPL cells (Agilent) as previously described (5). For the glycosylation reaction, purified CAPRIN1 was dialyzed into OGT reaction buffer (25 mM Tris, 50 mM NaCl, 0.5 mM EDTA, 2 mM DTT, pH 7.5). The final reaction mixture contained 10 μM CAPRIN1, 1 μM OGT, 1 mM uridine 5'-diphospho-N-acetylglucosamine (UDP-GlcNAc; Millipore-Sigma) in OGT reaction buffer. Following a 24 h incubation period at room temperature, the reaction was quenched by the addition of 2 M GuHCl and then concentrated in an Amicon centrifugal concentration unit equipped with a 3 kDa molecular-weight-cutoff membrane. The concentrated sample was injected onto a Superdex 75 16/60 column equilibrated with gel filtration buffer (50 mM Tris, 500 mM NaCl, 3 M GuHCl, and 2 mM β-mercaptoethanol, pH 7.4) to separate the *O*-GlcNAcylated CAPRIN1 from the enzyme and other reaction components. Fractions containing *O*-GlcNAcylated CAPRIN1 were

pooled and concentrated for storage. *O*-GlcNAcylation of CAPRIN-1 was validated by liquid chromatography coupled to electrospray mass spectrometry.

Production of NMR samples

(1) NMR samples measuring CAPRIN1 ATP interactions

In order to probe binding of ATP to CAPRIN1, several 400 μM U-^{15}N, ^{13}C-labeled CAPRIN1 samples were prepared, dissolved in 25 mM HEPES, pH 7.4, 98% H_2O/2% D_2O. These included a pair of samples to which 1.6 mM ATP-Mg + 1% Mn^{2+} (*i.e.*, 16 μM Mn^{2+}) or 1.6 mM ATP-Mg was added (Fig. 1*C*, black). A second pair of samples was prepared consisting of either just CAPRIN1, or CAPRIN1 to which 5.6 μM Mn^{2+} was added, which serves as a control to evaluate spurious Mn^{2+} binding in the absence of ATP (Fig. 1*C*, green). The amount of Mn^{2+} added corresponds to the concentration of free Mn^{2+} (*i.e.*, not bound to ATP) in the 1.6 mM ATP-Mg + 16 μM Mn^{2+} sample based on K_D values for Mg^{2+} and Mn^{2+} binding to ATP of 10.3 and 67.1 μM, respectively, measured via ITC. Similar samples were generated for the experiments of Fig. 6*D*, except that 70 mM ATP-Mg was used. It is worth noting that in all experiments involving ATP, pH = 7.4 samples were used (as opposed to lower pH samples when amide proton-based experiments were recorded) to ensure the physiological ATP charge state (-4). Although highly sensitive fluorescence imaging experiments (Fig. 1A,B) showed that phase separation occurs under the conditions used to record NMR spectra in Figure 1C and Figure 2 (measurement of inter-molecular NOEs in mixed-state samples, see immediately below), the concentration of added ATP was such that sample turbidity could not be observed by the naked eye, indicating that the bulk of the protein is not phase separated, so that high quality NMR datasets can be recorded on mixed-state protein samples at the CAPRIN1/ATP ratios used. Notably, when the

sample becomes highly phase separated it is obvious, with extensive turbidity; in our studies visual differences could not be observed between mixed-state samples with or without ATP.

(2) NMR samples for measurement of NOEs

Inter-molecular NOEs (with and without 0.8 mM ATP, Fig. 2*B*-*F*) were recorded on mixed-state samples comprising 0.5 mM concentrations each of $^{13}C,^{1}H$- and $^{12}C,^{1}H$-labeled CAPRIN1, dissolved in buffer composed of 15 mM Tris (D11, 98%), pH 7.4, with 100% D_2O as solvent.

The approach used to make the CAPRIN1 condensed-phase samples follows the protocol described in detail previously (2). NMR samples used for measurement of NOEs comprised a 1:2 ratio of mixtures of ^{12}C, ^{15}N, ^{2}H:^{13}C, ^{14}N, ^{1}H labeled CAPRIN1 (inter-molecular, Fig. 3*B*, *D*, and *E*, and Fig. 4*A* and *B*) or a 1:5 molar ratio of ^{13}C, ^{15}N, ^{1}H:^{12}C, ^{14}N, ^{1}H labeled CAPRIN1 (intra-molecular, Fig. 5*A* and *B*), 400 mM NaCl, 25 mM MES, pH 5.5, 90%H_2O,10%D_2O (condensed phase NMR buffer). In the inter-molecular class of experiment optimal signal-to-noise is achieved using samples with equal concentrations of the two differentially labeled polypeptides (see above), but the sensitivity decreases slowly with changes in relative amounts of the two components, while the cost of producing per-deuterated protein increases linearly with protein concentration so that a 1:2 ratio was used as a compromise. As a control, a phase-separated sample was also constructed to establish that the observed NOEs in the 1:2 ^{12}C, ^{15}N, ^{2}H:^{13}C, ^{14}N, ^{1}H mixture were of the inter-molecular variety (*i.e.*, that there were no/few spurious H^C-H^N intra-molecular NOEs from the ^{13}C, ^{14}N, ^{1}H component; *SI Appendix*, Fig. S6). This sample was composed of 1:2 ^{12}C, ^{14}N, ^{1}H:^{13}C, ^{14}N, ^{1}H labeled CAPRIN1. Based on the phase diagrams of Figure 3A, the CAPRIN1 concentration in the condensed phase is 248 mg/mL, 40^{o}C, corresponding to 22.4 mM in protein. 3 mm NMR tubes were used to minimize the required

volumes and hence the amount of protein. Intra-chain NOE experiments (Fig. 5*A*) were also recorded on a mixed-state CAPRIN1 sample, 2 mM in protein, mixed-state NMR buffer, 4^{o}C (200 ms mixing time).

^{15}N spin relaxation experiments (Fig. 5, *C* and *D*) were recorded on the condensed phase using the 1:2 ^{12}C, ^{15}N, ^{2}H:^{13}C, ^{14}N, ^{1}H labeled CAPRIN1 sample or on U-^{15}N-,^{13}C-labeled mixed-state samples with concentrations varying from 2 mM to 100 μM, mixed-state NMR buffer, with 2% D_2O, as described below.

NMR spectroscopy

Binding of ATP-Mn to CAPRIN1 (Fig. 1*C*, and 6*D*) was measured from peak volume changes in 3D haCONHA spectra, correlating $^{1}H^{\alpha}$, ^{13}CO chemical shifts of residue j with the backbone amide ^{15}N shift of residue j+1 (2). Datasets were collected using non-uniform sampling (NUS) as described previously (2) and processed using SMILE (6) that is part of the nmrPipe package (7). Acquisition times of 65 ms (^{13}CO) and 55 ms (^{15}N) were employed, with 10% of the indirect (^{13}CO,^{15}N) data points recorded, 12 scans/FID, and a relaxation delay (d1) of 1s, for a net acquisition time of 13 h/3D. The use of H^{α}-based experiments is particularly important as the sample pH is 7.4, resulting in poor quality H^{N}-observe spectra. Similarly, *O*-GlcNAcylation of CAPRIN1 was monitored by recording a series of 3D haCONHA spectra spaced 6.5 h apart to establish the time-course of the reaction. Chemical shift perturbations based on spectra recorded before addition of enzyme and 33 hours after the start of the reaction were used to establish which serine residues were glycosylated (Fig. 6*A*).

Inter-molecular NOEs in mixed-state 0.5 mM ^{13}C,^{1}H- and 0.5 mM ^{12}C,^{1}H-labeled CAPRIN1 samples (Fig. 2*B*-*F*; ±ATP-Mg) were recorded at 600 MHz, 25^{o}C, with the

edited/filtered pulse scheme of Zwahlen *et al.* (8), with the exception that the filtering/editing steps were reversed as described by Kumar *et al*. (9). Briefly, a double purge element is applied at the end of the pulse scheme, of purge durations 4.4 ms and 4.0 ms, using 60 kHz swept (upfield to downfield and centered at 0 ppm) ^{13}C adiabatic pulses of durations 2.359 and 1.536 ms, respectively (amplitude of 5 kHz). In addition, a third purge element (applied immediately after the first pair) of duration 4 ms was employed. Each of the 3D datasets was recorded with acquisition times of 40 ms, 5.6 ms and 80 ms in indirect ^{1}H, indirect ^{13}C, and direct ^{1}H dimensions using NUS where 25% of the indirect data was sampled. A 250 ms mixing time was used along with d1 = 1.5 s, for a total acquisition of time of approximately 3 days/experiment.

A series of five different 2D NOE-based ^{15}N-^{1}H^{N} HSQC experiments were recorded to measure inter- and intra-chain contacts in the condensed phase using pulse schemes outlined in *SI Appendix*, Fig. S4. Datasets were recorded using gradient selected TROSY schemes (10) with an ^{15}N indirect dimension acquisition time of 45 ms, d1 = 1.5 s, and 48 scans/FID for an acquisition time of approximately 4.5 hours per experiment. Complete sets of experiments were obtained with mixing times of 100 and 200 ms, except for the control experiments (to ensure that intra-molecular NOEs were not observed in inter-molecular NOE spectra) where datasets with a 200 ms mixing time only were recorded. 3D datasets were obtained for measuring methyl-^{1}H^{N} NOEs, recorded with acquisition times of 8 ms and 45 ms in ^{13}C and ^{15}N dimensions, respectively, 4 scans/FID and d1=1.5 ms, for a net acquisition time of ~1.5 days/spectrum. For these experiments (both inter- and intra-molecular NOEs) gradient, sensitivity enhanced HSQC (11) readouts were used. All NOE data were recorded on a Bruker AVANCE NEO 23.4 T (1 GHz) spectrometer, equipped with an x,y,z gradient TCI cryoprobe, 40°C.

Intra-molecular NOEs were also recorded on a mixed-state CAPRIN1 sample (2 mM, 4°C, 600 MHz) using identical pulse schemes as for the condensed phase, with the exception that the readout was a sensitivity enhanced HSQC (*i.e.*, non-TROSY). NOE experiments were recorded on a Bruker AVANCE III 14.0 T (600 MHz) spectrometer, equipped with an x,y,z gradient TCI cryoprobe, using a mixing time of 200 ms.

^{15}N R_1 and $R_{1\rho}$ relaxation rates were recorded on a condensed-phase sample of CAPRIN1 comprising a 1:2 ratio of ^{12}C, ^{15}N, ^{2}H:^{13}C, ^{14}N, ^{1}H labeled molecules (40°C), as well as on U-^{15}N,^{13}C 2 mM, 250 μM, and 100 μM samples of WT mixed-state CAPRIN1 or 100 μM samples of mutants of mixed-state CAPRIN1 (4°C, to maximize intra-chain contacts). Standard TROSY-based (condensed phase) (12) or gradient enhanced sensitivity based (mixed state) HSQC experiments (13) were used, recorded on either Bruker AVANCE III HD 14.0 T or AVANCE NEO 23.4 T spectrometers. A series of 7 time points extending from 5 ms – 125 ms (mixed state) or 5 ms – 100 ms (condensed phase) was collected for measurement of $R_{1\rho}$, while 6 time points (10 ms – 700 ms) were obtained for measurement of R_1 relaxation rates. Transverse relaxation rates, R_2, were calculated from the relation (14)

$$R_2 = (R_{1\rho} - R_1\cos^2\theta) / \sin^2\theta \qquad [1]$$

where $\theta = \arctan(v_1/\Delta\Omega)$, v_1 is the spin-lock field strength (2 kHz), and $\Delta\Omega$ is the offset (Hz) of the spin in question from the carrier (14). ^{1}H-^{15}N NOE experiments were recorded as described previously (15) using a pair of experiments recorded with (i) a pre-scan delay of 8 s followed by presaturation for 6 s or (ii) 14 s of presaturation, achieved using the method of Ferrage *et al* (16).

All NMR data were processed using the NMRPipe processing package and analyzed using routines in NMRPipe (7) and in NMRFAM-Sparky (17). Peak intensities were quantified

in 3D datasets by using the nlinLS fitting routine in NMRPipe; intensities in 2D data were obtained by using the Peakipy software package (https://github.com/j-brady/peakipy).

CAPRIN1 chemical shift assignment

Backbone chemical shifts of CAPRIN1 in the mixed state were assigned using standard triple resonance experiments (18), and subsequently transferred to spectra of the condensed CAPRIN1 phase. This was readily accomplished as peaks shifted by only small amounts. In order to verify the transferred assignments, a 3D HNCO dataset was recorded of condensed-phase CAPRIN1. Figure S2 shows a 2D ^{15}N-$^{1}H^{N}$ TROSY HSQC of the condensed phase of CAPRIN1, 40°C, 1 GHz, with assignments as indicated.

Supplementary Information Text

Rationale behind NMR approach

NMR studies of intrinsically disordered proteins (IDPs) and intrinsically disordered regions (IDRs) of otherwise folded proteins are challenged by poor spectral resolution, especially in applications focusing on sidechain interactions (4, 19). A case in point is provided by ^{13}C-edited/filtered experiments (8) that quantify inter-molecular NOEs (Fig. 2). Although residue-specific interactions can be established, site-specific contacts in IDRs and IDPs are more difficult to discern because aliphatic/aromatic ^{13}C and ^{1}H resonance frequencies associated with a given position in an amino acid are localized to very narrow regions of chemical shift space (20). In principle, sidechain information can be forthcoming in disordered systems so long as magnetization can be transferred to backbone ^{15}N or ^{13}CO spins that are better resolved than other heteronuclei (21, 22). This is often possible in studies of mixed-state solutions of IDPs or IDRs (*i.e.*, not condensed phases of phase-separated samples) since their intrinsic backbone and

sidechain dynamics leads to increased relaxation times that can be leveraged to enable efficient transfer of magnetization between spins in a scalar-coupled spin system, even when the couplings are small (23, 24). Elegant CON experiments have emerged whereby both ^{13}CO and ^{15}N frequencies are recorded to generate well-resolved correlation maps of intrinsically disordered systems (25). Although such experiments are predicated on lengthy magnetization transfer steps connecting ^{13}CO and ^{15}N spins and, often, additional transfers to sequential residues (26–29), sensitivity is usually not an issue and the spectral resolution afforded is excellent. Applications involving protein molecules in the condensed phase of phase-separated systems face more challenges because the high viscosity of the samples and contributions from chemical exchange lead to a significant increase in transverse relaxation rates, and, thus, concomitant decreases in magnetization transfer efficiencies (4). Thus, although it is easy to envision NOE experiments in which inter-molecular contacts 'become resolved' by recording backbone ^{15}N and ^{13}CO chemical shifts, in practice such experiments are of poor quality because magnetization transfer steps are lossy. Our strategy is therefore one of compromise. Because inter-molecular NOEs in condensed-phase samples of IDPs/IDRs are weak, since interactions are, in general, transient, it is necessary to minimize magnetization transfers so as to optimize sensitivity. We have, therefore, focused on the measurement of inter-molecular NOEs connecting aromatic protons or certain aliphatic protons with backbone amide protons, exploiting the fact that ^{15}N chemical shifts are dispersed even in IDPs (30), so that well-resolved 'read-outs' of the NOE can be obtained. We are interested in key residues, such as Phe/Tyr/Arg that have been identified to be important for LLPS in this work (Fig. 2) and in previous studies of CAPRIN1 (1, 2) and other proteins (4, 31–34), as well as backbone α-protons. Therefore, sensitive 2D experiments have been developed to excite proton spins in a residue-specific

(Aromatic/Arg/Gly/Ser) manner, or specifically the α-protons of all non-Gly residues; magnetization from such spins is then transferred to backbone amides via the NOE and quantified by recording ^{15}N-$^{1}H^{N}$ TROSY (or non-TROSY) based HSQC pulse schemes. By using a 1:2 ratio of ^{12}C, ^{15}N, ^{2}H: ^{13}C, ^{14}N, ^{1}H labeled molecules, high sensitivity 2D inter-molecular NOE data sets can be recorded in 2 hours on our samples (although typically we recorded 4-5 hour experiments) so that a suite of five experiments can be obtained in a day of instrument time. In principle, it is possible to measure a 4D dataset that provides similar information. In practice, the 40% reduction in sensitivity with each increasing dimension, along with relaxation losses associated with the additional acquisition times, is not inconsiderable. As a limited number of spin-types are examined (corresponding to five experiments), we prefer the 2D approach. Figure S4 shows pulse sequence diagrams for the NOE experiments that have been designed. Selective inversion of the aromatic/aliphatic proton spins of interest is accomplished through the use of INEPT magnetization transfer elements to create ^{1}H-^{13}C longitudinal order from initial ^{1}H polarization that is subsequently manipulated, and then refocused back to longitudinal ^{1}H magnetization prior to an NOE mixing period. Finally, magnetization is recorded using an ^{15}N-$^{1}H^{N}$ HSQC readout so that NOEs can be quantified. Manipulation of magnetization to achieve selection occurs (i) during evolution in the INEPT periods and/or (ii) by the application of selective pulses (often both ^{1}H and ^{13}C) during intervals where ^{1}H-^{13}C longitudinal order is present, so as to minimize relaxation losses. Optimal selection efficiencies vary from > 95% (aromatics) to 83%-90% for the remaining experiments (although in the Ser datasets recorded in the present work, selection was less efficient, 65%, due to a less than optimal width of the adiabatic decoupling elements during the first INEPT; see *SI Appendix*, Fig. S4). In all of the profiles presented (Fig. 4, 5, and *SI Appendix*, Fig. S9) NOE intensities have not been

normalized to take into account differences in efficiencies by which protons were selected. In order to optimize selection of the magnetization of interest, we have also developed simple ^{13}C-^{1}H HSQC experiments whereby the sequences of *SI Appendix*, Fig. S4 are modified by removing the mixing period and subsequent ^{1}H-^{15}N HSQC block and changing the phase of the ^{1}H 90° pulse immediately preceding the mixing period from y to x. The resulting ^{13}C-edited 1D ^{1}H spectrum (or 2D ^{13}C-^{1}H correlation map) can be used to evaluate selectivity and sensitivity, with the frequency position of the selective pulses optimized to achieve excitation of the desired spins, while minimizing sensitivity losses. *SI Appendix*, Fig. S3 shows 2D ^{13}C-^{1}H HSQC spectra, illustrating that excellent selectivity is, in general, achieved for the five experiments of interest.

Studying condensed protein phases at 1 GHz *vs* lower fields

There are a number of important advantages associated with using ultra-high magnetic fields (in our case 1 GHz) in studies of IDPs or IDRs of proteins that reflect the improved resolution (proportional to B_o^N, where N is the dimensionality of the experiment, neglecting the potential effects of conformational exchange), as well as the increased TROSY effect that is predicted to be optimal in the vicinity of 1 GHz (35). The improved resolution between 600 MHz and 1 GHz in studies of the condensed phase of CAPRIN1 can be substantial (*SI Appendix*, Fig. S2*E*). Nevertheless, there is a tradeoff. While contributions to R_2 from exchange are likely to be small for mixed-state samples, larger contributions may be expected in applications involving condensed phases. In order to explore this more fully, we have recorded ^{15}N R_1, R_2 and ^{1}H-^{15}N NOEs on samples of 2 mM CAPRIN1 (4°C, mixed phase) and 1:2 ^{12}C, ^{15}N, ^{2}H: ^{13}C, ^{14}N, ^{1}H CAPRIN1 (40°C, condensed phase) at static magnetic fields of 14.0 (600 MHz) and 23.4 T (1 GHz) and carried out a spectral density mapping analysis so as to separate contributions to R_2

from chemical exchange (R_{ex}) and ns-ps timescale dynamics. The approach followed that of Farrow *et al* (36) and assumed that R_{ex} scales as B_o^2. An ^{15}N-$^{1}H^{N}$ bond vector length of 1.04 Å and an axially symmetric ^{15}N CSA value of -163 ppm (37) were used in the analysis. Notably, significant R_{ex} values were obtained for the condensed-phase sample, in particular in a region encompassing residues G620-R640 and R660-Q680, where R_{ex} (600 MHz) values are as large as 8 s^{-1} (22 s^{-1} at 1 GHz), *SI Appendix*, Fig. S2*D*. In contrast, much smaller values of R_{ex} (600 MHz) were extracted from a similar analysis of data collected on the mixed sample with $R_{ex} < 1$ s^{-1} for all but one residue (Y670, $R_{ex} = 1.7$ s^{-1}). Because of the high sensitivity of our experiments, in general, and the overall resolution gains we elected to record many of the experiments at the higher field, but the 'optimal' field strength is an important consideration that must be visited on a case-by-case basis.

Effects of spin-diffusion on CAPRIN1 inter-molecular NOE intensities

The inherent flexibility of IDRs and IDPs does not mean that magnetization transfer during NOE mixing periods cannot occur via spin diffusion in these dynamic systems. J(0) spectra density values for CAPRIN1 have been calculated from ^{15}N R_1, R_2 and ^{1}H-^{15}N NOEs, using the spectral density mapping approach, as described above, and are plotted as a function of residue in *SI Appendix*, Fig. S7*A*. $J(0) = 2/5 \times S^2\tau_c$ values on the order of 2 ns and 6 ns are obtained for mixed (4°C) and condensed-phase (40°C) CAPRIN1 samples, respectively, corresponding to $S^2\tau_c$ values (S^2 is the square of the backbone amide order parameter and τ_c is the site-specific effective correlation time) of 5 ns and 15 ns, respectively, or to folded proteins with molecular masses of approximately 10 kDa and 30 kDa. Deuteration can significantly mitigate spin-diffusion, in addition to providing significant sensitivity gains (*SI Appendix*, Fig. S2*C*), and we

exploit this in the construction of the condensed-phase sample for measurement of inter-molecular NOEs since one of the components is ^{12}C, ^{15}N, ^{2}H labeled. However, the second component is ^{13}C labeled and, of necessity, also protonated, so that spin diffusion pathways within this chain, and, in particular, within protons of a given sidechain, are certainly operative. Our comparative studies of intra- and inter-molecular NOEs in the condensed phase indicate that intra-residue NOEs (that are, of course, intra-molecular) can be an order of magnitude larger than inter-molecular contacts (compare Fig. 4*B* and 5*A*). Thus, it is likely that in the Aro experiment, for example, a fraction of the magnetization will be transferred directly from $H^{\delta/\varepsilon/\zeta}$ to H^{N} on a neighboring chain, with an additional magnetization component diffusing rapidly up the aromatic sidechain via a multi-step process prior to transferring to the neighboring H^{N}. In order to evaluate these scenarios quantitatively we have recorded the Aro experiment as before except that an aliphatic ^{1}H selective pulse (900 μs Iburp (38), centered at 2.9 ppm, 1 GHz), was applied in the middle of the mixing period. The effect is to invert aliphatic ^{1}H magnetization, leaving amide and aromatic ^{1}H spins unchanged, thereby removing the spin diffusion pathway that proceeds through a magnetization transfer process that can be described schematically as $H^{\delta/\varepsilon/\zeta} \xrightarrow{\text{intra}} H^{\alpha/\beta} \xrightarrow{\text{inter}} H^{N}$, where "intra" and "inter" above the arrows indicate intra-residue and inter-molecular magnetization transfer during the mixing period, respectively, and $H^{\alpha/\beta}$ denotes H^{α} or H^{β} protons of the same residue. This approach is analogous to that suggest originally by Massefski and Redfield (39) and to the QUIET-NOESY schemes that were subsequently developed by Bodenhausen and coworkers (40). Figure S7B shows 1D traces from the Aro-NOE experiment recorded with and without the selective aliphatic ^{1}H pulse at mixing times of 100 and 200 ms, showing that approximately 30% (100 ms) and 45%-50% (200 ms) of the net $H^{\delta/\varepsilon/\zeta}$ to H^{N} inter-molecular magnetization transfer occurs via multiple steps involving

aliphatic protons, very likely along the aromatic sidechain. Very similar spectra are obtained when one or a pair of selective pulses (uniformly spaced) is applied during the mixing period, or when the selective pulse inverts the aromatic and amide protons, rather than the aliphatic spins, that also suppresses spin diffusion pathways through aliphatic protons. Figure S7C plots normalized NOE intensities (100 ms mixing time) as a function of the backbone amide position obtained in the Aro-NOE experiment recorded with the selective aliphatic pulse, establishing that very similar profiles are obtained with or without (*i.e.*, severely attenuated) spin-diffusion pathways.

Comparison of intra- and inter-molecular NOE intensities

Our data establish that intra-molecular NOEs in the CAPRIN1 condensed-phase sample, primarily localized to intra-residue and sequential residue interactions, are significantly more intense (by as much as an order of magnitude) than the corresponding inter-molecular contacts that extend over much larger regions of sequence. As the intra- and inter-molecular NOE experiments were recorded on separate NMR samples in order to ensure the appropriate magnetization transfer pathways (see Fig. 3*B*), it is important to consider differences in sample concentrations in an evaluation of the relative magnitudes of NOEs in each case, and to establish whether inter-molecular NOEs would be expected to be observed in the "intra-molecular NOE" condensed-phase sample. As described in the text, we have used a sample comprised of a 1:2 ratio of ^{12}C, ^{15}N, ^{2}H: ^{13}C, ^{14}N, ^{1}H labeled CAPRIN1 molecules to record inter-molecular NOEs. At 40°C, the concentration of protein in the condensed phase is 22.4 mM (Fig. 3*A*) so that the two components have concentrations of ~7.5 mM (^{12}C, ^{15}N, ^{2}H) and ~15 mM (^{13}C, ^{14}N, ^{1}H). In order to calculate the effective concentration of protein that gives rise to inter-molecular NOEs,

we consider a simple model whereby magnetization is transferred between a pair of proximal (^{13}C, ^{14}N, ^{1}H:^{12}C, ^{15}N, ^{2}H) chains. At any given time, proximal chains can be (^{13}C, ^{14}N, ^{1}H:^{13}C, ^{14}N, ^{1}H), (^{12}C, ^{15}N, ^{2}H:^{12}C, ^{15}N, ^{2}H), or (^{13}C, ^{14}N, ^{1}H:^{12}C, ^{15}N, ^{2}H), with probabilities of 4/9, 1/9, and 4/9, respectively, and with effective concentrations of 5, 1.25, and 5 mM, respectively. Thus, inter-molecular NOEs derive from pairs of chains with an effective concentration of 5 mM. It is worth noting that to optimize the inter-molecular NOE intensities a sample with equal concentrations of labeled components is required, to produce an effective concentration of 5.6 mM for 'NOE-active' pairs of proximal (^{12}C, ^{15}N, ^{2}H: ^{13}C, ^{14}N, ^{1}H) proteins, approximately 12% higher than what was used here.

As described in the text, a second sample that was labeled as 1:5 ^{13}C, ^{15}N, ^{1}H:^{12}C, ^{14}N, ^{1}H CAPRIN1 was prepared to record intra-molecular contacts in the condensed phase. The effective concentration of 'intra-molecular NOE active molecules' is, therefore 3.7 mM (1/6 x 22.4 mM), that is slighter lower than for the inter-molecular NOE measurements (effective concentration of 5 mM). Although it is possible to produce a sample that is heavily biased towards 'generating' intra-molecular NOEs, by using a skewed ratio of ^{13}C, ^{15}N, ^{1}H:^{12}C, ^{14}N, ^{1}H molecules, there can, nevertheless, be inter-molecular NOE transfer involving pairs of proximal ^{13}C, ^{15}N, ^{1}H chains. Following arguments given above, an effective concentration of (^{13}C, ^{15}N, ^{1}H: ^{13}C, ^{15}N, ^{1}H) pairs, giving rise to inter-molecular NOEs, of 0.3 mM is calculated, over an order of magnitude lower than the concentration of ^{13}C, ^{15}N, ^{1}H CAPRIN1 from which intra-molecular correlations are generated (3.7 mM), and over 15-fold less than the effective concentration for measurement of inter-molecular NOEs in the 1:2 ^{12}C, ^{15}N, ^{2}H: ^{13}C, ^{14}N, ^{1}H labeled sample. Thus, inter-molecular contacts in the 'intra-NOE' sample are expected to be much smaller than their intra-NOE counterparts, and very likely not visible (*SI Appendix*, Fig. S8).

In order to rigorously compare NOEs within a given experiment (intra or inter) we have normalized their intensities with the corresponding intensities of amide correlations in HSQC experiments, as described in the text. In this manner peak broadening due to conformational exchange (*SI Appendix*, Fig. S2*D*) or exchange with water that would otherwise give rise to residue specific changes in NOE intensities are taken into account. Normalization with respect to HSQC intensities is even more important in a comparison of intra- and inter-molecular NOEs, as different samples are used that are labeled in different ways (^{15}N,^{2}H for inter and ^{15}N,^{1}H for intra). Taking into account the difference in the effective protein concentrations that gives rise to intra- and inter-molecular NOEs, 3.7 mM and 5 mM, respectively (see above), and the concentration differences of the ^{15}N-labeled CAPRIN1 components that produce the HSQC spectra used to normalize the measured NOEs (3.7 mM and 7.5 mM for intra- and inter-molecular NOEs), the normalized inter-molecular NOEs must be multiplied by a factor of 1.5 (7.5/5) to be fully comparable with their intra-molecular NOE counterparts. We have not "normalized" the reported NOE values in this way, however, as the factor is relatively small compared to the very significant differences that are observed between the inter- and intra-molecular classes of NOE.

Finally, unlike in studies of the intra-molecular condensed-phase sample (1:5 ^{13}C, ^{15}N, ^{1}H: ^{12}C, ^{14}N, ^{1}H CAPRIN1), inter-molecular NOEs are expected in the H^C to H^N NOE experiments of *SI Appendix*, Fig. S4 using the mixed-state 2 mM U-^{15}N,^{13}C CAPRIN1 sample, although intra-NOEs will be much more intense. Figures 5A (right) and S8 (bottom) make the point clearly, showing that measured NOEs in the mixed-state sample are predominantly of the intra- and sequential residue variety, while significantly weaker inter-molecular NOEs are observed that span 10-20 residues (*SI Appendix*, Fig. S8). Note that the mixed-state sample was placed in a 5

mm NMR tube, while 3 mm tubes were used for all condensed-phase samples. Based on the protein concentrations and labeling of each sample, and taking into account the increase in signal from using a 5 mm relative to a 3 mm tube (that is expected to scale with volume for low salt samples), we calculate an increase of 9-fold for inter-molecular NOEs in the mixed-state sample relative to the 1:5 ^{13}C, ^{15}N, ^{1}H: ^{12}C, ^{14}N, ^{1}H condensed-phase sample, neglecting other factors.

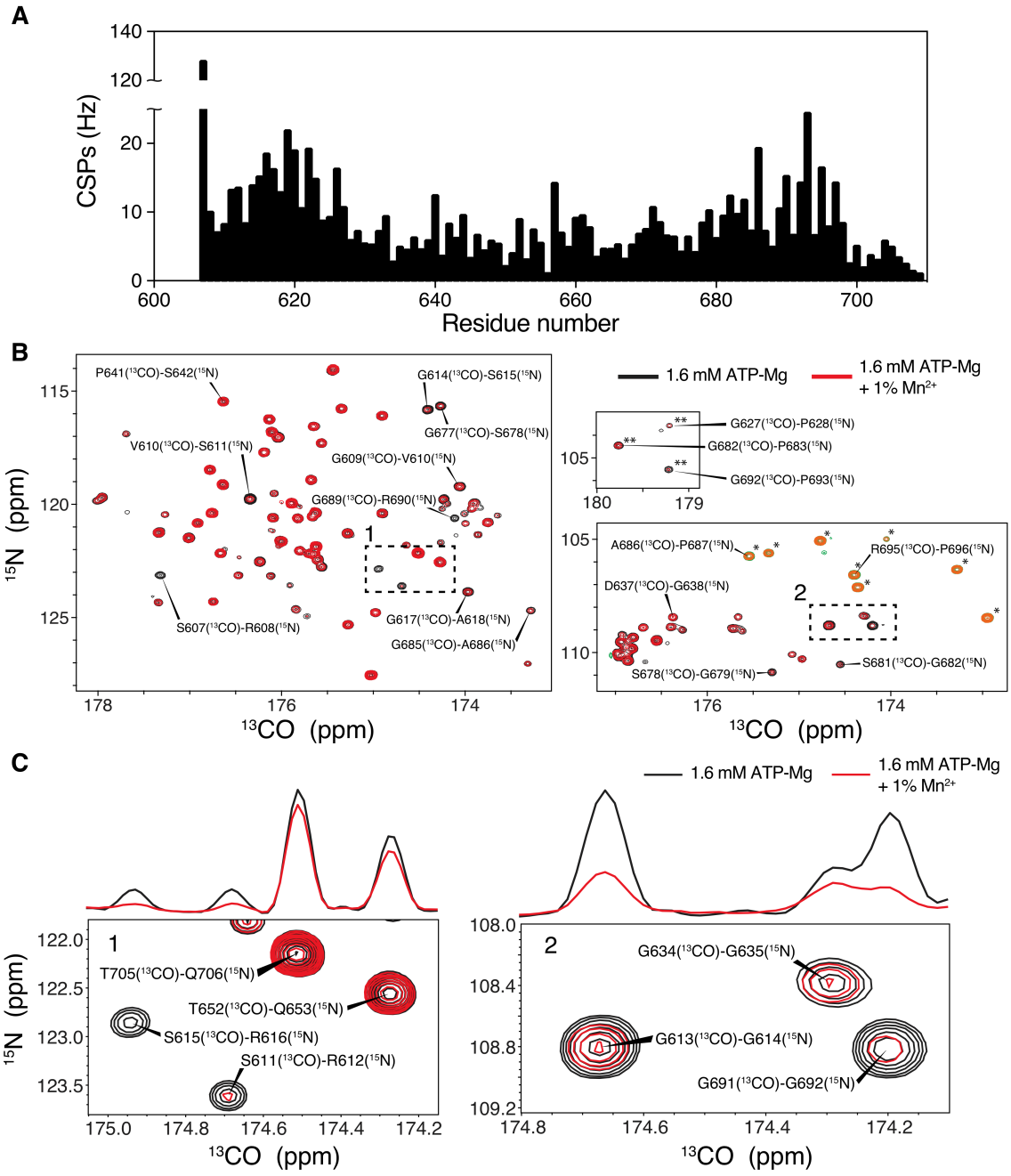

Fig. S1. ATP binds to Arg-rich sequences of CAPRIN1. (**A**) Chemical shift perturbations (CSPs) upon binding of ATP-Mg to CAPRIN1 at pH 7.4, 25°C. CSPs were calculated using the following equation, $\mathrm{CSP} = \sqrt{\Delta\nu_{^1H\alpha}{}^2 + \Delta\nu_{^{13}CO}{}^2 + \Delta\nu_{^{15}N}{}^2}$, where $\Delta\nu$ is the difference (Hz) between peak positions in 3D haCONHA datasets recorded with and without 1.6 mM ATP-Mg. (**B**) Selected regions of 2D ^{15}N-^{13}CO projections from 3D haCONHA datasets recorded on U-^{15}N-,^{13}C-labeled mixed-state CAPRIN1 samples, 1.6 mM ATP-Mg, in the presence (red) or absence (black) of 1% Mn^{2+} (600 MHz, 25°C). Peaks connecting (^{13}CO, $^1H^{\alpha}$; residue j) to ^{15}N of Pro (residue j+1) are aliased (shown in green for 1.6 mM ATP-Mg and orange for 1.6 mM ATP-Mg

+ 1% Mn^{2+}, and indicated by *), while peaks connecting Gly-Pro are doubly aliased (small panel centered at 105 ppm (^{15}N) and 179.5 ppm (^{13}CO) and indicated by **). Some assignments are shown. (**C**) Expanded views of selected spectral regions from (B) showing attenuation of peak intensities in regions where ATP-Mn binds. Shown above each spectral region are 1D ^{13}CO projections, calculated as sums over the ^{15}N dimension. Note that a control experiment establishes that no loss in signal intensity occurs when 5.6 μM Mn^{2+} is added in the absence of nucleotide, corresponding to the concentration of free Mn^{2+} in the ATP-Mg + 1% Mn^{2+} sample. This establishes that the attenuation is due to binding of ATP-Mn (Fig. 1*C*).

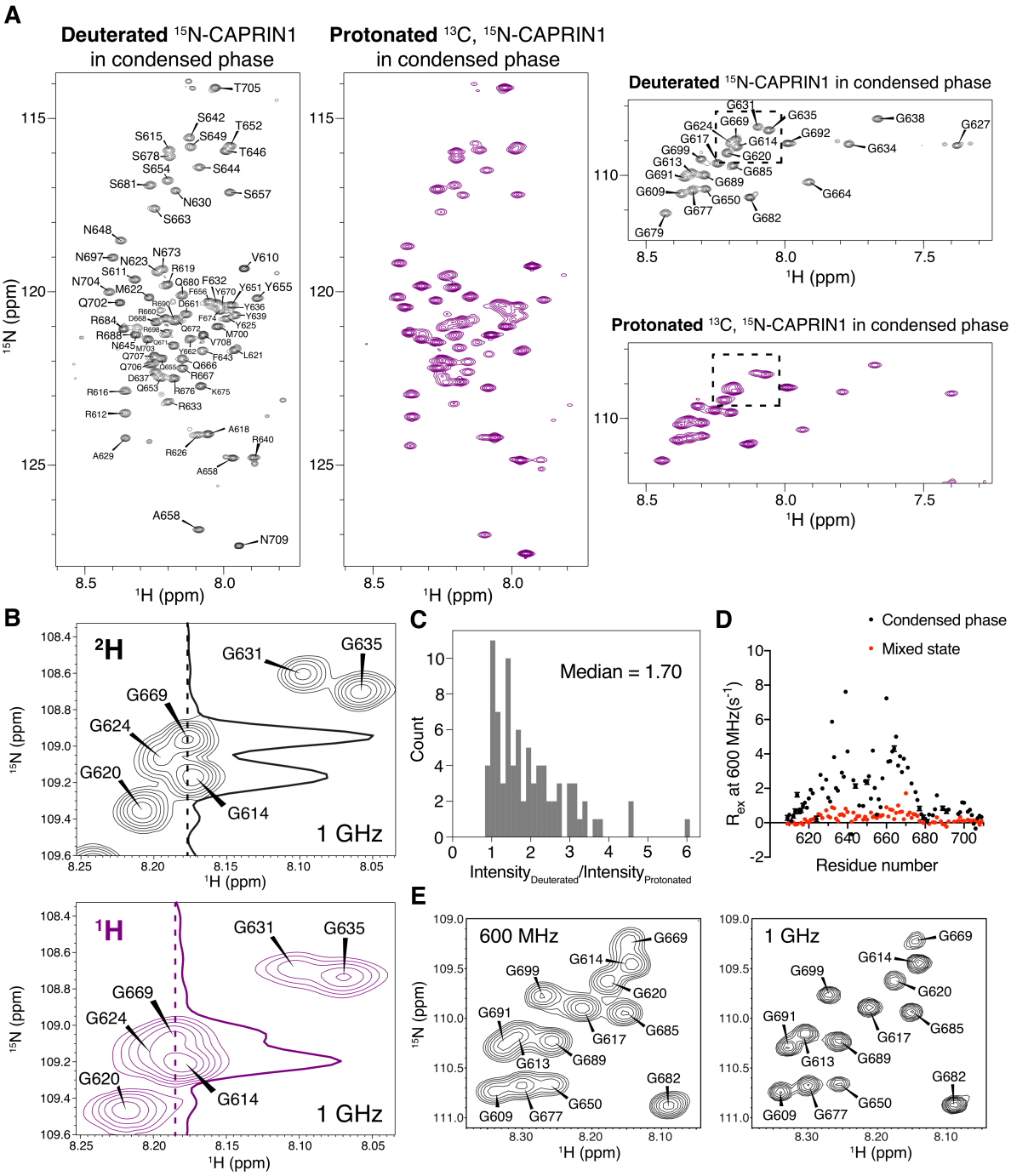

Fig. S2. Resolution and sensitivity enhancement of condensed-phase spectra by deuteration and improvements at 1 GHz. (**A**) Comparison of ^{15}N-^{1}H^{N} TROSY-HSQC spectra of 1:2 ^{12}C, ^{15}N, ^{2}H: ^{13}C, ^{14}N, ^{1}H and 1:5 ^{13}C, ^{15}N, ^{1}H:^{12}C, ^{14}N, ^{1}H CAPRIN1 condensed-phase samples (used for the measurement of inter- and intra-molecular NOEs, respectively, 40°C, 1 GHz), with assignments as indicated. (**B**) Enlarged spectral region from ^{2}H- (top, black) and ^{1}H- (bottom, purple) labeled ^{15}N chains (inter- and intra-molecular NOE samples, respectively), illustrating the improved spectral resolution that deuteration affords. (**C**) Histogram showing the intensity

ratios of peaks in ^{15}N-$^{1}H^{N}$ TROSY-HSQC spectra of ^{12}C, ^{15}N, ^{2}H- and ^{13}C, ^{14}N, ^{1}H-CAPRIN1 in the condensed phase, accounting for differences in sample concentrations. The median improvement in sensitivity with deuteration is 1.7-fold (40°C, 1 GHz). (**D**) Resolution in spectra of condensed-phase proteins can be negatively affected due to exchange contributions to transverse relaxation rates. Comparison of R_{ex} values (exchange contributions to R_2 at 600 MHz) for condensed-phase (40°C) and mixed-state (4°C) samples based on a spectral density mapping analysis (36) using relaxation data recorded at 14.0 and 23.4 T (see description above). It is important to note that $R_{1\rho}$ rates were recorded with an ^{15}N spin-lock field of 2 kHz and thus exchange contributions with lifetimes in excess of approximately 500 μs contribute little to the measured R_{ex} values. Therefore, contributions from exchange during free-precession periods would be expected to be larger than the values indicated. R_{ex} rates at 1 GHz can be calculated by multiplying R_{ex}(600MHz) by 100/36. (**E**) Comparison of Gly spectral regions from ^{15}N-$^{1}H^{N}$ TROSY-HSQC spectra of 1:2 ^{12}C, ^{15}N, ^{2}H: ^{13}C, ^{14}N, ^{1}H condensed phase CAPRIN1 at 600 MHz (left) and 1 GHz (right), 40°C, establishing significant resolution benefits for the dataset recorded at 1 GHz. Contour levels are adjusted to have similar numbers of contours in both spectra. These spectra were recorded after the sample had aged such that the G624 cross-peak had shifted in position due to formation of an iso-Asp linkage involving N623-G624 (2).

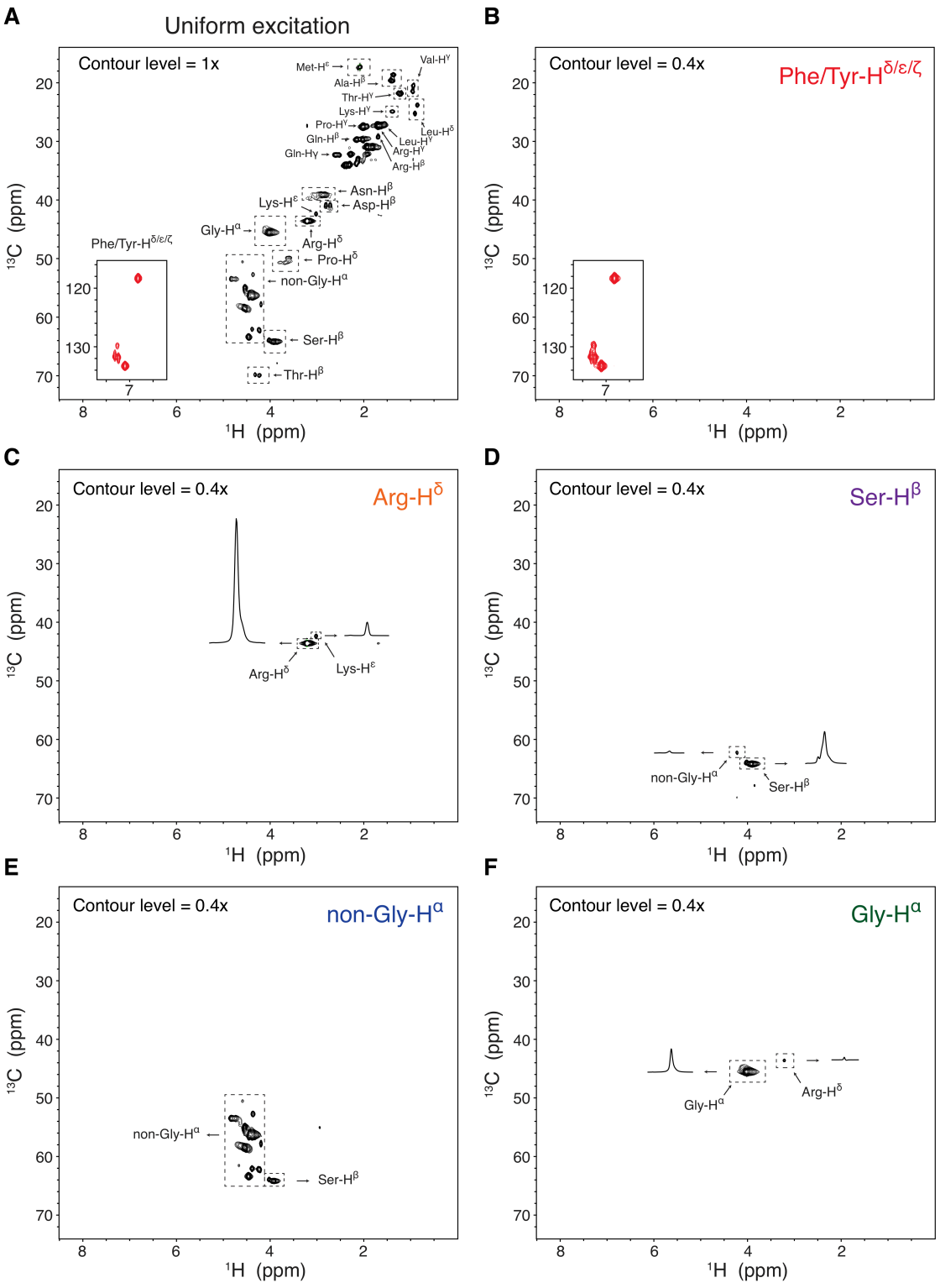

Fig. S3 Spectral editing of H^C (Phe/Tyr $H^{\delta/\varepsilon/\zeta}$, Arg H^{δ}, Ser H^{β}, non-Gly H^{α}, Gly H^{α}) protons for measurement of intra-/inter-molecular NOEs. (**A**) ^{13}C-^{1}H correlation map of condensed-phase CAPRIN1 (40°C, 600 MHz). The peaks derived from aromatic residues are aliased in the

^{13}C dimension. ^{13}C-^{1}H correlation maps, selectively editing for (**B**) Phe/Tyr-H$^{\delta/\varepsilon/\zeta}$ (no other aromatic residue types in CAPRIN1), (**C**) Arg-H$^{\delta}$, (**D**) Ser-H$^{\beta}$, (**E**) non-Gly-H$^{\alpha}$, and (**F**) Gly-H$^{\alpha}$, using the pulse schemes of *SI Appendix*, Fig. S4, modified to record ^{13}C,^{1}H maps. Contour levels in spectra shown in (B)-(F) are lowered by 2.5-fold relative to (A) to highlight the level of selectivity in each class of experiment.

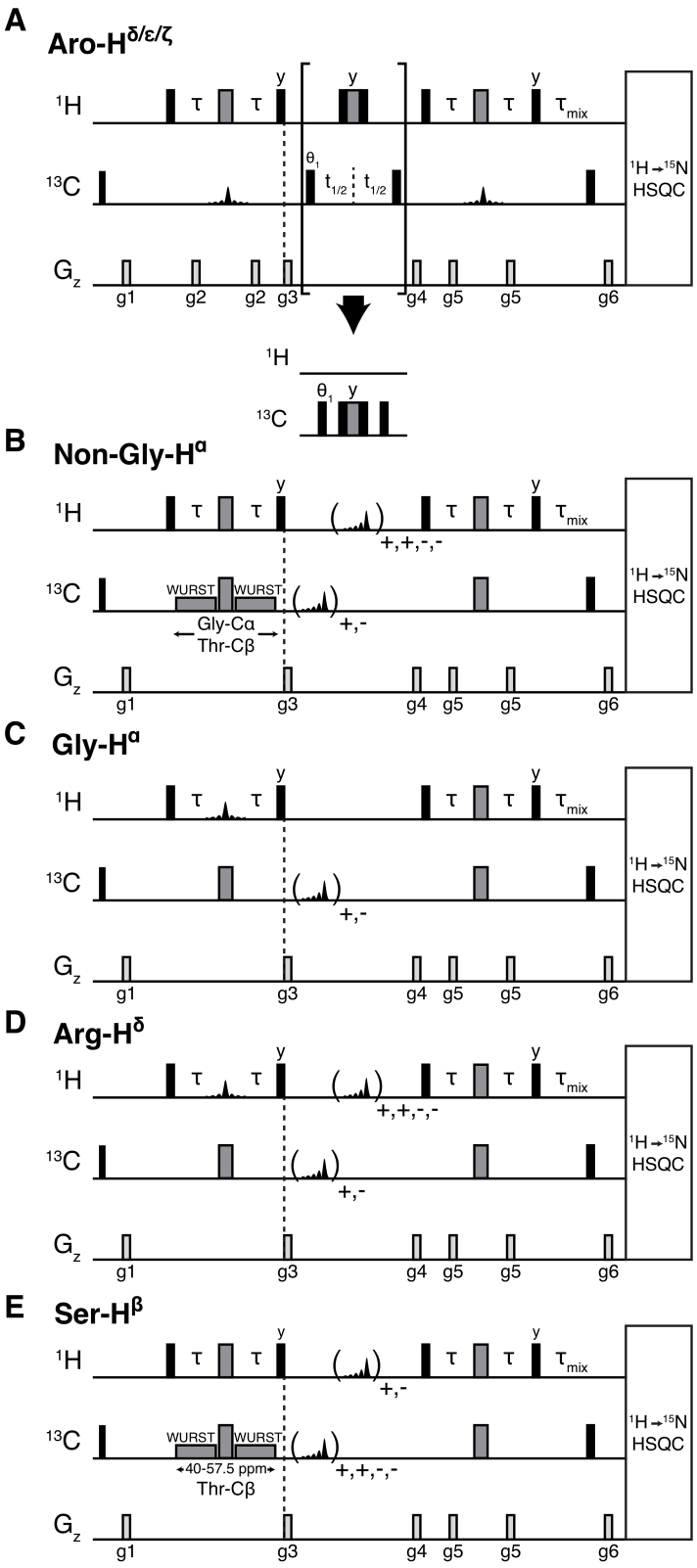
A
Aro-Hδ/ε/ζ
1H
13C
Gz
τ
τmix
y
θ1
t1/2
1H→15N HSQC
g1
g2
g3
g4
g5
g6
B
Non-Gly-Hα
WURST
Gly-Cα
Thr-Cβ
+,+,-,-
+,-
C
Gly-Hα
D
Arg-Hδ
E
Ser-Hβ
40-57.5 ppm

Fig. S4. Pulse schemes used to select for ^{1}H spins of interest (*i.e.*, aromatic spins in the Aro experiment, all H^α with the exception of α-protons from Gly in the Non-Gly-H^α experiment and so forth). The ^{1}H carrier is positioned on the water signal for the duration of the pulse scheme (including HSQC portion), while the ^{13}C carrier is placed at a frequency indicated below and subsequently jumped between C^α and CO spins, 117 ppm, during the HSQC element. All rectangular ^{1}H and ^{13}C pulses are applied at the highest possible power settings, and ^{1}H and ^{13}C black(grey) rectangular pulses have 90°(180°) flip angles. The HSQC 'box' at the end of each scheme denotes either a TROSY-based HSQC sequence (35), which has been used in the majority of the experiments, or an enhanced sensitivity HSQC sequence (11). Gradient strengths (in % maximum) and durations are: g1=(10%,1ms), g2=(20%,0.3ms), g3=(35%,0.8ms), g4=(-40%,0.8ms), g5=(-10%,0.3ms), g6=(30%,0.6ms). Selective pulse durations correspond to those used for recording spectra at a static magnetic field of 23.4T (1 GHz) and can be adjusted for any B_o field according to the relation: pulse duration(B_o) = pulse duration(1GHz) x B_o(1GHz)/B_o. (**A**) Pulse scheme for selecting aromatic protons. The ^{13}C carrier is positioned at 125 ppm and aromatic protons are selected by applying 510 μs on-resonance ^{13}C pulses with the REBURP profile (38) during INEPT and reverse-INEPT transfers (41), τ = 1.6 ms. The phase ϕ_1 is cycled ±x with concomitant inversion of the receiver phase. The experiment can be measured in 3D mode by including an extra dimension whereby aromatic ^{13}C chemical shifts are recorded (t_1) with quadrature in this indirect dimension achieved via STATES-TPPI (42) of phase θ_1; in 2D mode the t_1 element is replaced by the inset shown below. This scheme has also been used to measure methyl-$^1H^N$ NOEs. In this case the ^{13}C carrier was positioned at 21 ppm, the REBURP pulses were of duration 1020 μs, τ = 1.8 ms, and 3D spectra were recorded. Notably, there is only a single Leu residue and some of the other methyl groups are sufficiently well resolved in the ^{13}C dimension so that site-specific information for both the origination and destination of magnetization is available in some cases. (**B**) Non-Gly-H^α experiment for measuring NOEs between α-protons of all residues, with the exception of Gly, and H^N spins. The ^{13}C carrier is positioned at 57.9 ppm, τ = 1.75 ms. A 1.38 ms ^{13}C IBURP pulse (38) is applied in alternate scans (indicated by +,- in the figure, where +(-) denotes application(absence) of the pulse), in concert with inversion of the phase of the receiver, to select for all C^α spins (except Gly). In order to eliminate contributions from Pro residues and most, but not all Ser residues, a 6 ms ^{1}H IBURP pulse centered at 3.6 ppm (center of Pro) is applied for the first 2 of every 4 scans (indicated in the figure by +,+,-,-), with no change to the phase of the receiver. Finally, ^{13}C WURST adiabatic decoupling elements (43) centered at 70 ppm (±2 ppm bandwidth; Thr-C^β) and 44 ppm (±4 ppm; Gly-C^α) are applied during the INEPT element to suppress magnetization transfer from protons of Gly and Thr (H^β) to ^{13}C and hence eliminate NOEs from them. (**C**) Gly experiment for measuring NOEs between Gly H^α and H^N protons. The ^{13}C carrier is positioned at 46 ppm. Selection of Gly H^α is achieved through the use of a 1.8 ms ^{1}H REBURP pulse during the INEPT element (τ = 1.75 ms) whose position is carefully tuned (~ 5.15 ppm) so as to minimize selection of other ^{1}H spins and optimize sensitivity (using the ^{13}C-^{1}H HSQC variant, as discussed above) and by the application of a 6 ms IBURP pulse on ^{13}C (46 ppm) in successive scans with concomitant inversion of the phase of the receiver when the pulse is applied. (**D**) Pulse scheme for measurement of Arg H^δ-H^N NOEs. The ^{13}C carrier is placed at 43.6 ppm, the resonance frequency of the Arg C^δ carbons. Selection of Arg H^δ protons is achieved through the use of a ^{1}H 1.8 ms REBURP pulse centered at the Arg H^δ resonance frequency (3.3 ppm) during the INEPT transfer period (τ = 1.85 ms), as well as by 9 ms (43.6 ppm) and 6 ms (3.3 ppm) ^{13}C

and ^{1}H IBURP pulses, applied successively, and for the first 2 of every 4 scans, respectively. The receiver is cycled x,2(-x),x during this 4-step element. (**E**) Measurement of Ser H^{β}-H^{N} NOEs. The ^{13}C carrier is positioned at 64 ppm. ^{1}H magnetization one-bond coupled to carbon spins resonating between 40-57.5 ppm or between 68-72 ppm is selected against during the first INEPT period (τ = 1.75 ms) by a ^{13}C WURST decoupling element centered at 48.75 ppm (±8.75 ppm bandwidth) and 70 ppm (±2 ppm; Thr-C^{β}) to eliminate NOE contributions from most H^{α} protons and H^{β} protons of Thr. A 12 ms ^{1}H IBURP pulse centered on the Ser H^{β} (3.95 ppm in our case) is applied in successive scans with concomitant inversion of the receiver phase to select for Ser H^{β}, while Gly H^{α} protons are eliminated through the action of 1.5 ms ^{13}C IBURP centered at 48 ppm applied for the first 2 of 4 scans with no change to the phase of the receiver.

As discussed above, these sequences can be easily modified to record ^{13}C,^{1}H correlation maps or 1D ^{13}C-edited spectra (to test for the efficacy of the selection process) by changing the phase of the final ^{1}H pulse from y to x, followed by signal detection (*i.e.*, eliminating the remaining sequence). It is strongly recommended that 1D ^{13}C-edited experiments by used to optimize the position of selective pulses, that are likely to depend slightly on the sample and experimental conditions.

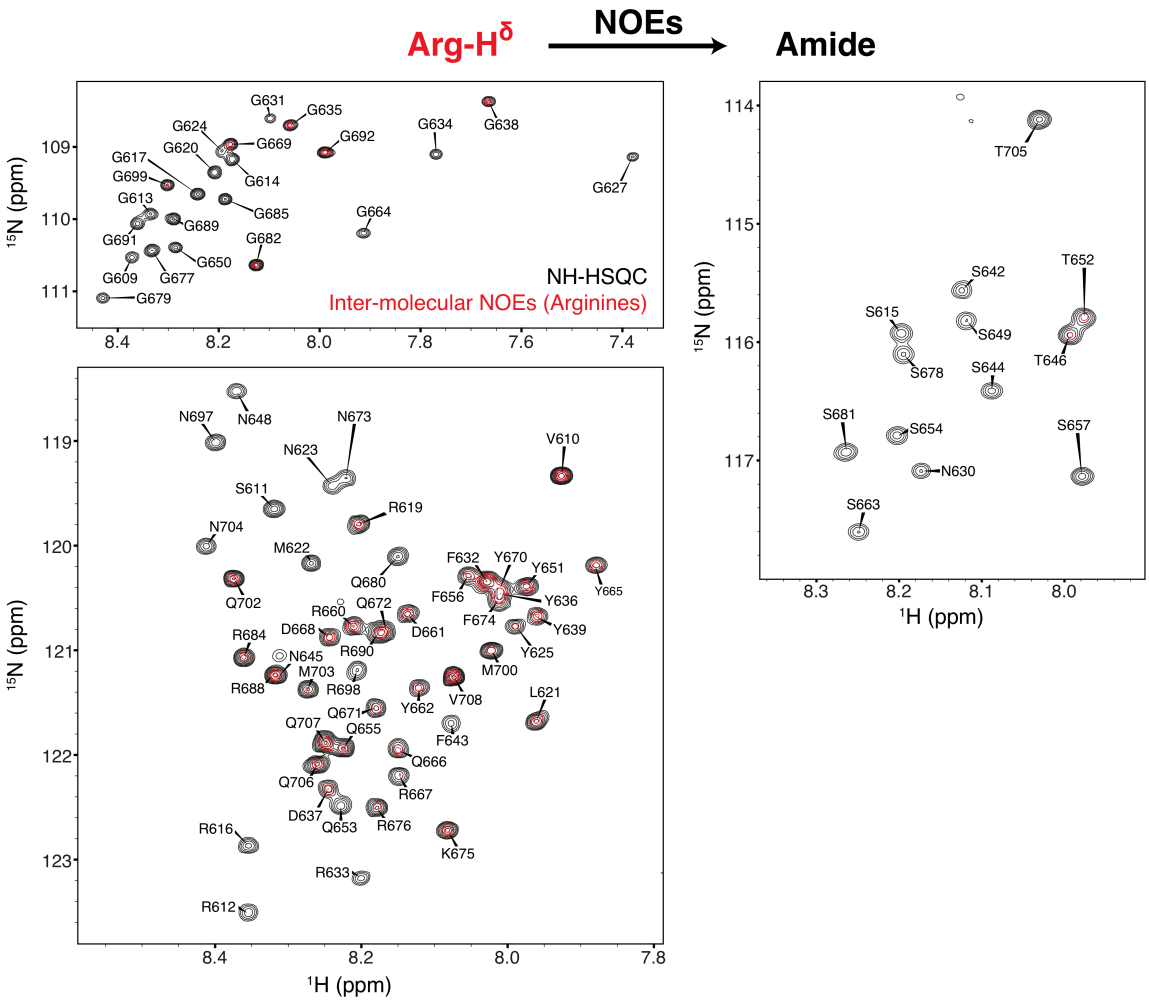

Fig. S5. Inter-molecular contacts between Arg H^{δ} and backbone amides in the condensed CAPRIN1 phase. Selected regions from a 200 ms NOESY dataset showing Arg H^{δ} - $^{1}H^{N}$ inter-molecular NOEs (red), superimposed on the corresponding regions from an HSQC-TROSY spectrum (black), recorded at 1 GHz, 40°C.

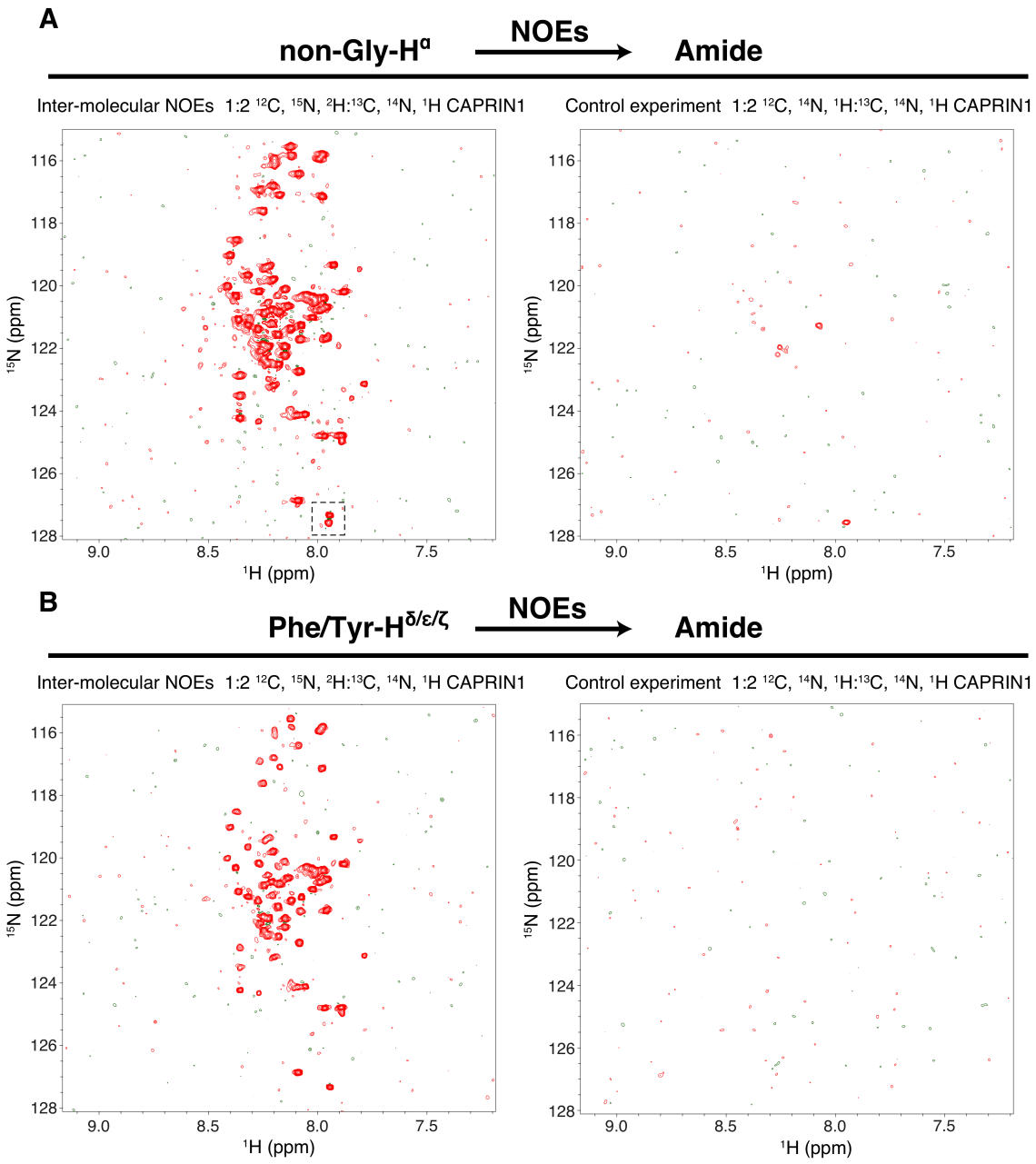

Fig. S6. Spurious intra-molecular NOEs are weak or not observed in the inter-molecular NOE experiment. (**A**) Comparison of non-Gly H^{α} NOE spectra recorded using 1:2 $^{12}C,^{15}N,^{2}H:^{13}C,^{14}N,^{1}H$ and 1:2 $^{12}C,^{14}N,^{1}H:^{13}C,^{14}N,^{1}H$ CAPRIN1 condensed-phase samples (40°C, 1 GHz, 200 ms mixing time). A large number of NOEs are observed using the 1:2 $^{12}C,^{15}N,^{2}H:^{13}C,^{14}N,^{1}H$ sample, as described in the text (left); although unlikely, some NOEs could, in principle, derive from an intra-molecular transfer within the $^{13}C,^{14}N,^{1}H$ chain, since in a natural abundance nitrogen sample ~0.3% of the nitrogen is ^{15}N. In order to evaluate whether this occurs, we have recorded corresponding datasets under identical conditions on a 1:2 $^{12}C,^{14}N,^{1}H:^{13}C,^{14}N,^{1}H$ CAPRIN1 sample (right). Of the 3 or 4 correlations (barely) above noise in the control spectrum for the non-Gly H^{α} experiment, the most sensitive of all NOE

experiments in our suite, one has an intensity of 12% and the remainder less than 8% of the corresponding peaks in the inter-molecular dataset. It is noteworthy that inter-molecular NOE correlations and spurious intra-molecular cross peaks are separated in positions by deuterium isotope shifts (44), as is shown in the dashed box where the upfield and downfield correlations derive from inter- (*i.e.*, to ^{2}H-protein) and intra- (*i.e.*, to ^{1}H-protein) NOEs. It is thus possible to separate the very few artifacts in the non-Gly H^{α} experiment (none are observed in any other experiments, see below) by the position of the peaks in the dataset. (**B**) Comparative Phe/Tyr-$H^{\delta/\varepsilon/\zeta}$-$H^{N}$ NOE spectra, as in (A). Spurious intra-molecular NOEs are not observed, nor are they observed in other NOE spectra.

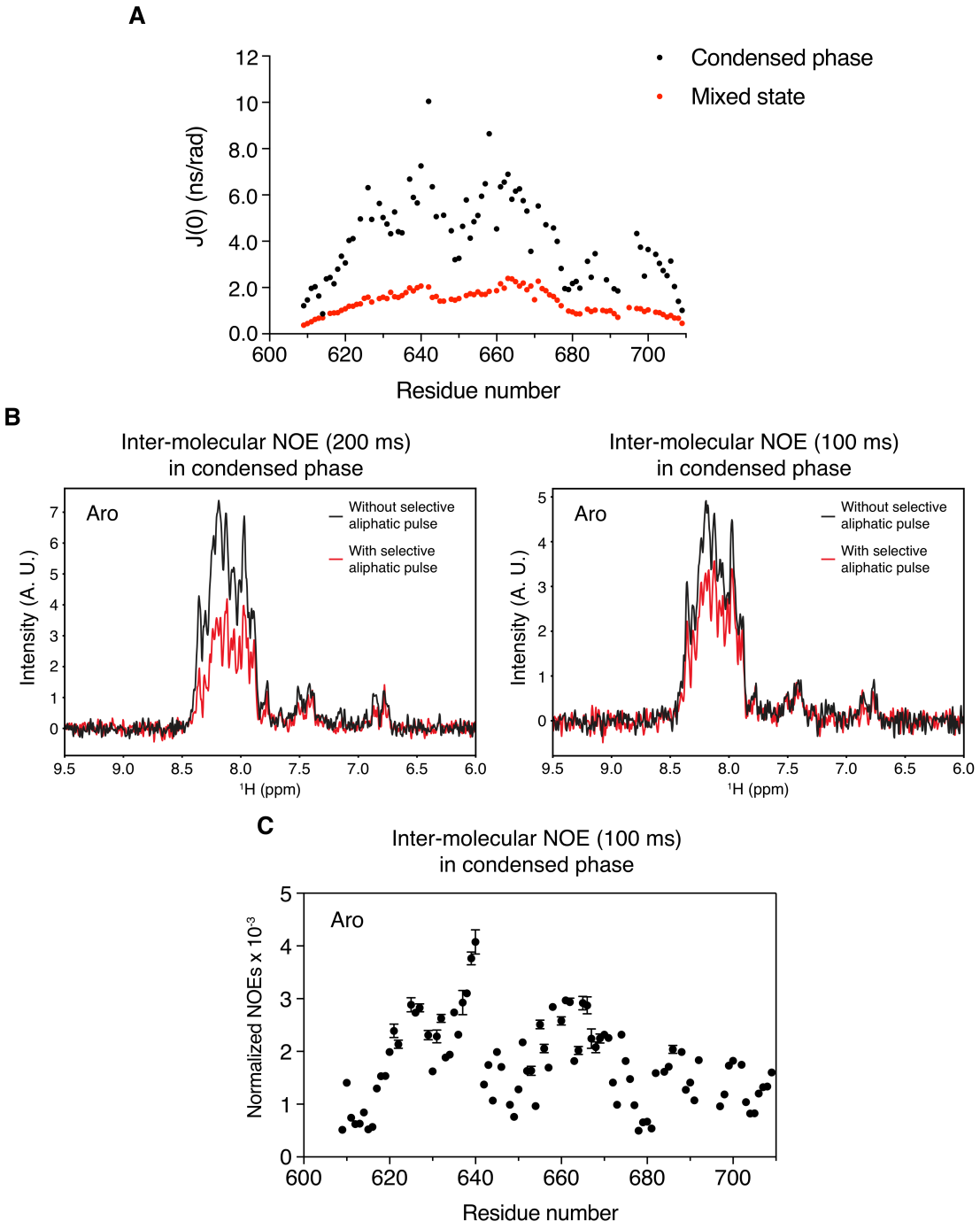

Fig. S7. Quantifying relative contributions to inter-molecular NOEs from direct and multi-step NOE magnetization transfer. (**A**) Plot of J(0) = 2/5 x $S^2\tau_c$ (45) as a function of residue for mixed-state (4°C) and condensed-phase (40°C) CAPRIN1 samples. (**B**) 1D NOE spectra corresponding to inter-molecular NOE transfer from aromatic $H^{\delta/\varepsilon/\zeta}$ protons to H^N of an adjacent chain with (red) or without (black) a ^1H aliphatic selective inversion pulse to minimize multi-step spin diffusion processes involving aliphatic protons. Approximately 30% (100 ms) and 50% (200

ms) of the net $H^{\delta/\varepsilon/\zeta}$ to H^{N} inter-molecular magnetization transfer occurs via multiple steps involving aliphatic spins, most likely along the aromatic sidechain. (**C**) Normalized NOE intensities as a function of backbone amide position, as Fig. 4*B*, obtained in the Aro experiment, 100 ms, recorded with a selective aliphatic pulse applied in the center of the mixing period. The same pattern as observed in the profiles of Fig. 4*B* is noted.

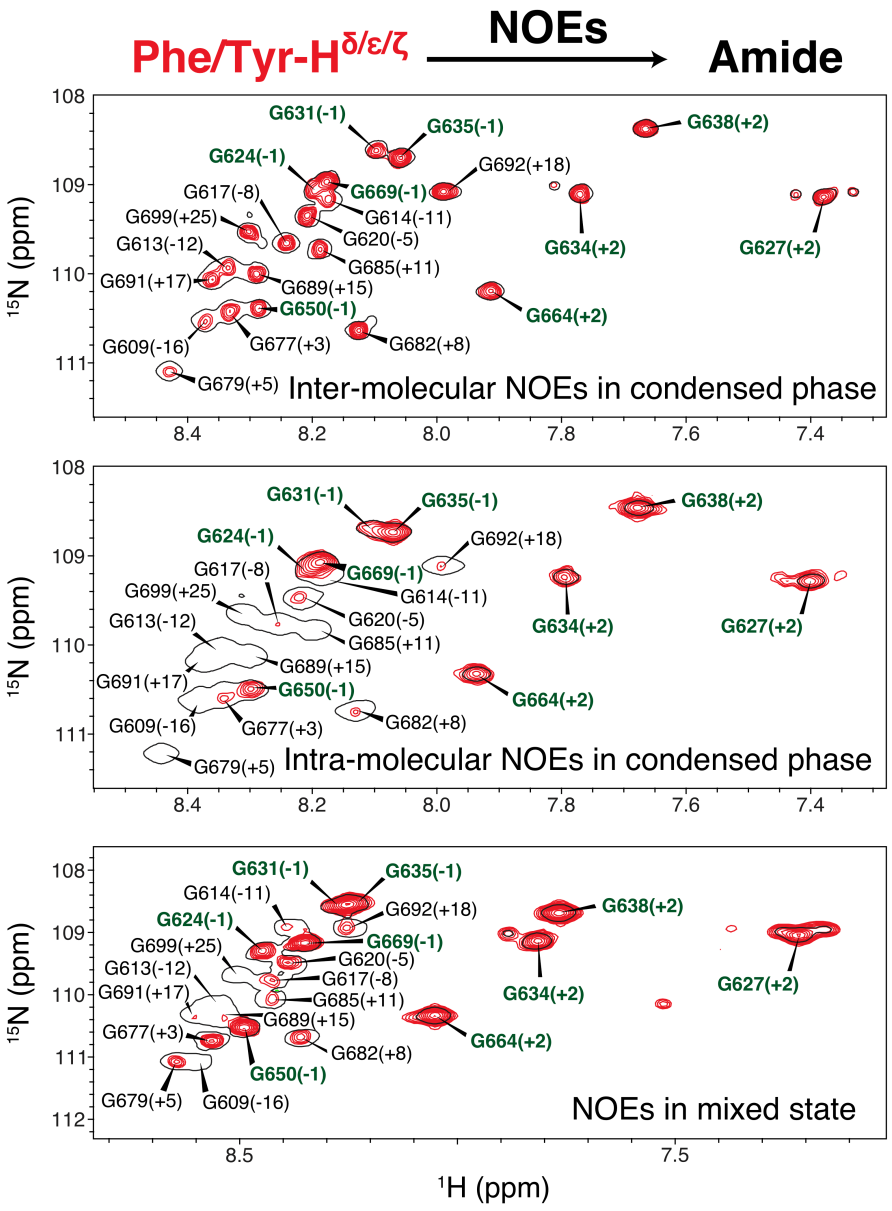

Fig. S8. Phe/Tyr-H$^{\delta/\varepsilon/\zeta}$-H^{N} NOEs from condensed and mixed-state CAPRIN1 samples show distinct patterns of inter- and intra-molecular NOEs. Selected regions of NOE datasets (highlighting NOEs to Gly amides) showing inter- and intra-molecular NOEs (red) from condensed-phase samples (top and middle, respectively; 40°C, 200 ms mixing time, 1 GHz), and NOEs from a mixed-state sample (bottom; 4°C, 200 ms mixing time, 600 MHz). NOEs from the mixed-state sample can be either intra- or inter-molecular, although those of the intra-molecular variety will be significantly more intense (see text above). Whereas intra-molecular NOEs are largely restricted to neighboring residues, highlighted in green, with the closest position relative to a Phe/Tyr indicated in brackets (+j indicates a Phe/Tyr residue j amino acids C-terminal to the Gly in question), inter-molecular contacts connect distal residues on separate chains. NOE spectra are shown as multiple contours with resonance assignments. Single black contours denote the positions of correlations in ^{15}N-^{1}H^{N} HSQC spectra.

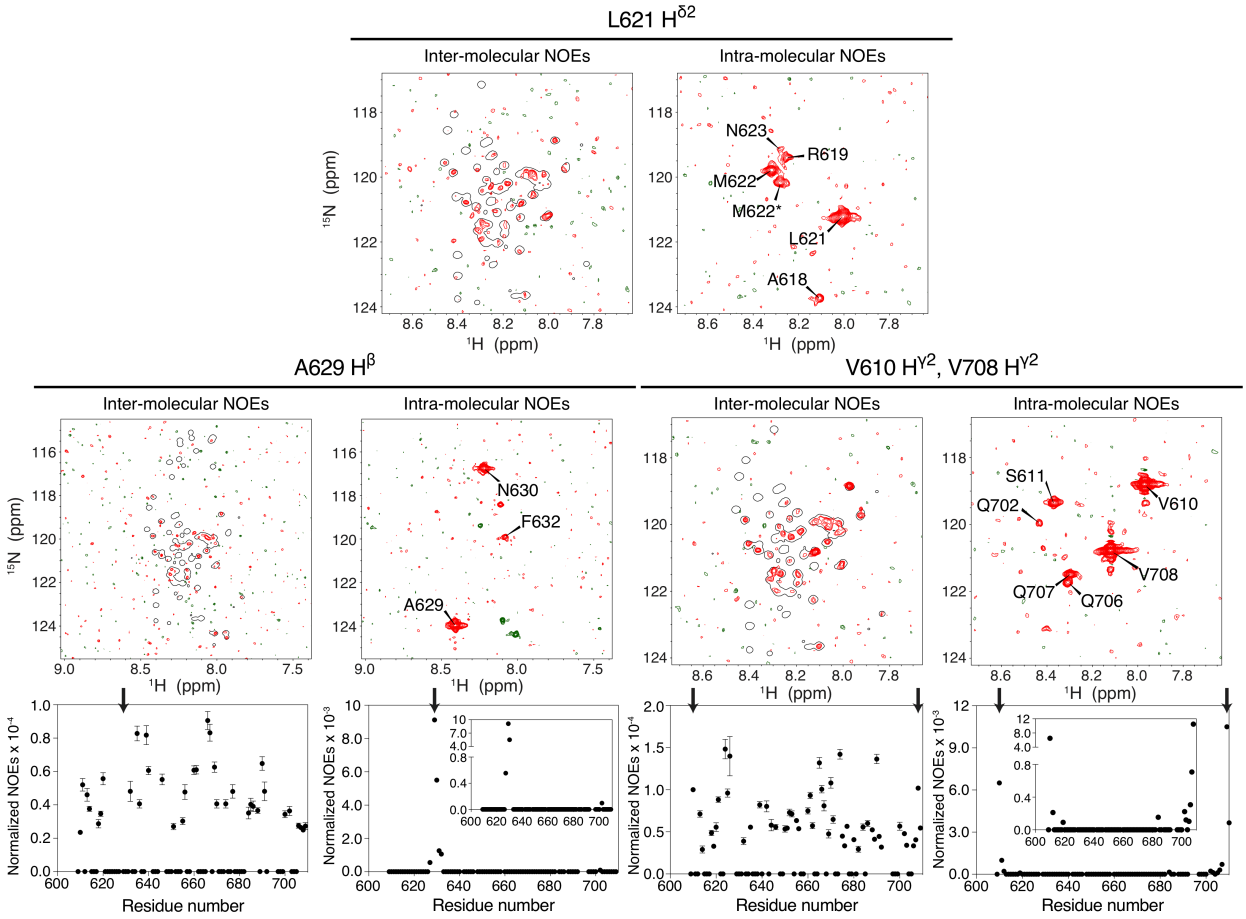

Fig. S9. Methyl-$^{1}H^{N}$ NOEs in the condensed CAPRIN1 phase emphasize differences between inter- and intra-molecular interactions. Comparison of inter- and intra-molecular, site-specific, methyl-amide NOEs observed in 1:2 ^{12}C, ^{15}N, ^{2}H:^{13}C, ^{14}N, ^{1}H and 1:5 ^{13}C, ^{15}N, ^{1}H:^{12}C, ^{14}N, ^{1}H labeled CAPRIN1 samples (200 ms mixing time, 40°C, 1 GHz), respectively. Single contours (black) highlight positions of amide correlations in ^{15}N-$^{1}H^{N}$ HSQC spectra, while red contours are NOEs. Planes from 3D NOE spectra are shown for L621 $H^{\delta2}$, A629 H^{β}, V610 $H^{\gamma2}$, and V 708 $H^{\gamma2}$, along with selected assignments. M622 and M622* denote correlations connecting L621 $H^{\delta2}$ with H^{N} of M622 where position 623 is asparagine or iso-aspartic acid (*), resulting from the slow deamidation of N623 (2). Arrows at the top of the profiles indicate the residue from which magnetization originates. Note that intensities of correlations from 3D NOE and 2D HSQC spectra were first normalized by measurement times of each dataset before calculating normalized NOE values. Contours are plotted at the noise level to establish that many of the correlations observed in the inter-molecular NOE dataset are not observed in the intra-molecular NOE spectrum.

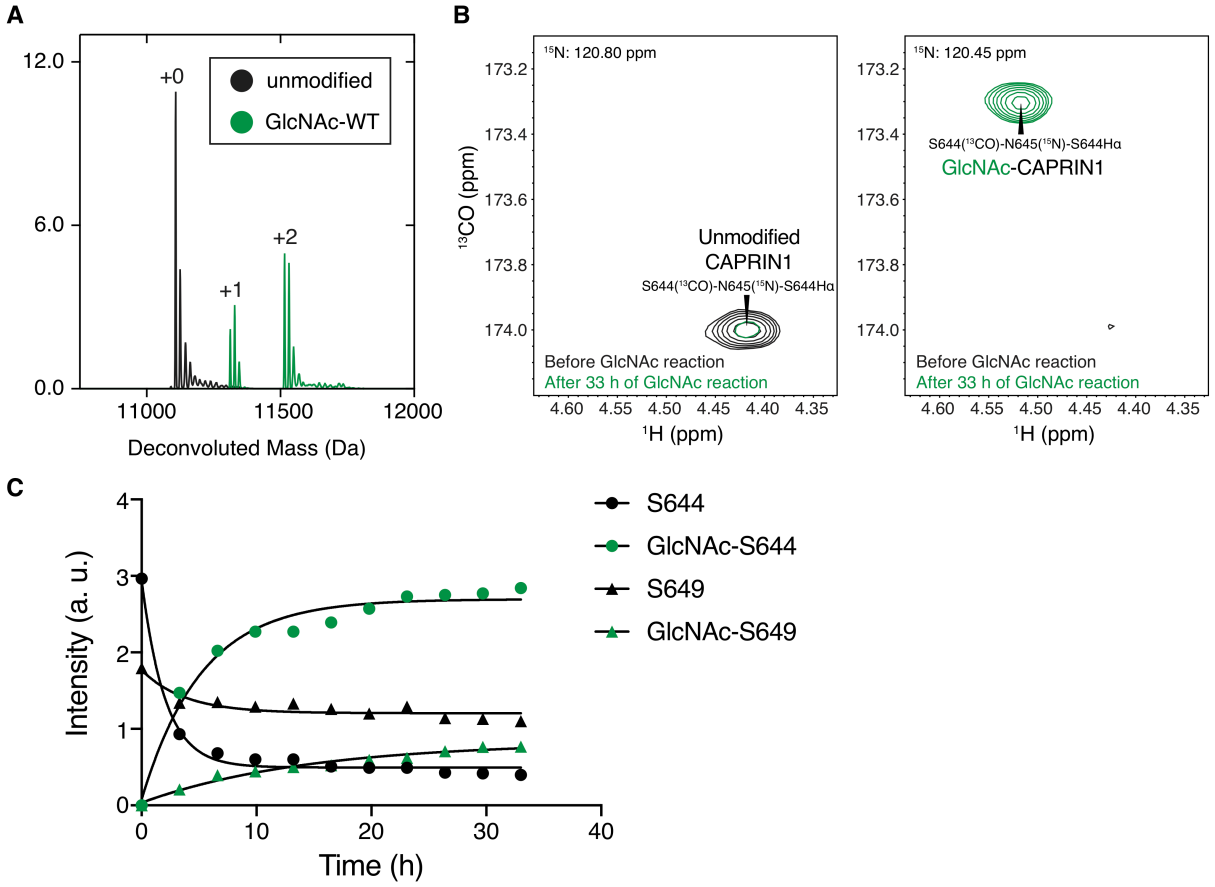

Fig. S10. *O*-GlcNAcylation of CAPRIN1 occurs at S644 and S649. (**A**) Mass spectrometry analysis of the CAPRIN1 *O*-GlcNAcylation reaction. Masses of unmodified CAPRIN1 (+0) and CAPRIN1 singly (+1) and doubly (+2) glycosylated (after 33 h of reaction) are shown. Multiple lines are observed for each species with a separation of either 16 or 32 Da, corresponding to oxidation of Met residues (there are 3 Met in the sequence) or addition of a sodium ion, respectively. (**B**) Selected planes from a 3D haCONHA data set (25°C, 600 MHz) showing the large change in corresponding peak positions that accompanies glycosylation at S644. (**C**) Time profile of the CAPRIN1 *O*-GlcNAcylation reaction (25°C) at positions S644 and S649, showing the build-up of new peaks from glycosylation (green) and decay of correlations that derive from the unmodified protein.

SI References

1. T. H. Kim, *et al.*, Phospho-dependent phase separation of FMRP and CAPRIN1 recapitulates regulation of translation and deadenylation. *Science* **365**, 825–829 (2019).
2. L. E. Wong, T. H. Kim, D. R. Muhandiram, J. D. Forman-Kay, L. E. Kay, NMR Experiments for Studies of Dilute and Condensed Protein Phases: Application to the Phase-Separating Protein CAPRIN1. *J. Am. Chem. Soc.* **142**, 2471–2489 (2020).
3. F. W. Studier, Protein production by auto-induction in high density shaking cultures. *Protein Expr. Purif.* **41**, 207–234 (2005).
4. J. P. Brady, *et al.*, Structural and hydrodynamic properties of an intrinsically disordered region of a germ cell-specific protein on phase separation. *Proc. Natl. Acad. Sci. U. S. A.* **114**, E8194–E8203 (2017).
5. B. J. Gross, B. C. Kraybill, S. Walker, Discovery of O-GlcNAc transferase inhibitors. *J. Am. Chem. Soc.* **127**, 14588–14589 (2005).
6. J. Ying, F. Delaglio, D. A. Torchia, A. Bax, Sparse multidimensional iterative lineshape-enhanced (SMILE) reconstruction of both non-uniformly sampled and conventional NMR data. *J. Biomol. NMR* **68**, 101–118 (2017).
7. F. Delaglio, *et al.*, NMRPipe: A multidimensional spectral processing system based on UNIX pipes. *J. Biomol. NMR* **6**, 277–293 (1995).
8. C. Zwahlen, *et al.*, Methods for measurement of intermolecular NOEs by multinuclear NMR spectroscopy: Application to a bacteriophage λ N-peptide/boxB RNA complex. *J. Am. Chem. Soc.* **119**, 6711–6721 (1997).
9. S. Kumar, *et al.*, The methyl ^{13}C-edited/^{13}C-filtered transferred NOE for studying protein interactions with short linear motifs. *J. Biomol. NMR* **74**, 681–693 (2020).
10. M. Salzmann, G. Wider, K. Pervushin, K. Wüthrich, Improved sensitivity and coherence selection for [^{15}N,^{1}H]-TROSY elements in triple resonance experiments. *J. Biomol. NMR* **15**, 181–184 (1999).
11. L. E. Kay, P. Keifer, T. Saarinen, Pure Absorption Gradient Enhanced Heteronuclear Single Quantum Correlation Spectroscopy with Improved Sensitivity. *J. Am. Chem. Soc.* **114**, 10663–10665 (1992).
12. N. A. Lakomek, J. Ying, A. Bax, Measurement of ^{15}N relaxation rates in perdeuterated proteins by TROSY-based methods. *J. Biomol. NMR* **53**, 209–221 (2012).
13. N. A. Farrow, *et al.*, Backbone Dynamics of a Free and a Phosphopeptide-Complexed Src Homology 2 Domain Studied by ^{15}N NMR Relaxation. *Biochemistry* **33**, 5984–6003 (1994).
14. A. G. Palmer, C. D. Kroenke, J. P. Loria, "Nuclear magnetic resonance methods for quantifying microsecond-to-millisecond motions in biological macromolecules" in *Methods in Enzymology*, (2001), pp. 204–238.
15. D. F. Hansen, *et al.*, An exchange-free measure of ^{15}N transverse relaxation: An NMR spectroscopy application to the study of a folding intermediate with pervasive chemical exchange. *J. Am. Chem. Soc.* **129**, 11468–11479 (2007).
16. F. Ferrage, A. Piserchio, D. Cowburn, R. Ghose, On the measurement of ^{15}N-{^{1}H} nuclear Overhauser effects. *J. Magn. Reson.* **192**, 302–313 (2008).
17. W. Lee, M. Tonelli, J. L. Markley, NMRFAM-SPARKY: Enhanced software for biomolecular NMR spectroscopy. *Bioinformatics* **31**, 1325–1327 (2015).
18. M. Sattler, J. Schleucher, C. Griesinger, Heteronuclear multidimensional NMR

experiments for the structure determination of proteins in solution employing pulsed field gradients. *Prog. Nucl. Magn. Reson. Spectrosc.* **34**, 93–158 (1999).
19. A. C. Murthy, *et al.*, Molecular interactions underlying liquid−liquid phase separation of the FUS low-complexity domain. *Nat. Struct. Mol. Biol.* **26**, 637–648 (2019).
20. D. S. Wishart, B. D. Sykes, Chemical shifts as a tool for structure determination. *Methods Enzymol.* **239**, 363–392 (1994).
21. W. Y. Choy, D. Shortle, L. E. Kay, Side chain dynamics in unfolded protein states: An NMR based ^{2}H spin relaxation study of Δ131Δ. *J. Am. Chem. Soc.* **125**, 1748–1758 (2003).
22. O. Zhang, J. D. Forman-Kay, D. Shortle, L. E. Kay, Triple-resonance NOESY-based experiments with improved spectral resolution: Applications to structural characterization of unfolded, partially folded and folded proteins. *J. Biomol. NMR* **9**, 181–200 (1997).
23. B. Brutscher, *et al.*, "NMR methods for the study of instrinsically disordered proteins structure, dynamics, and interactions: General overview and practical guidelines" in *Advances in Experimental Medicine and Biology*, (Springer New York LLC, 2015), pp. 49–122.
24. Y. Yoshimura, N. V. Kulminskaya, F. A. A. Mulder, Easy and unambiguous sequential assignments of intrinsically disordered proteins by correlating the backbone ^{15}N or ^{13}C' chemical shifts of multiple contiguous residues in highly resolved 3D spectra. *J. Biomol. NMR* **61**, 109–121 (2015).
25. W. Bermel, I. Bertini, I. C. Felli, R. Kümmerle, R. Pierattelli, Novel ^{13}C direct detection experiments, including extension to the third dimension, to perform the complete assignment of proteins. *J. Magn. Reson.* **178**, 56–64 (2006).
26. D. Pantoja-Uceda, J. Santoro, New ^{13}C-detected experiments for the assignment of intrinsically disordered proteins. *J. Biomol. NMR* **59**, 43–50 (2014).
27. M. G. Murrali, *et al.*, ^{13}C APSY-NMR for sequential assignment of intrinsically disordered proteins. *J. Biomol. NMR* **70**, 167–175 (2018).
28. I. C. Felli, R. Pierattelli, S. J. Glaser, B. Luy, Relaxation-optimised Hartmann-Hahn transfer using a specifically Tailored MOCCA-XY16 mixing sequence for carbonyl-carbonyl correlation spectroscopy in ^{13}C direct detection NMR experiments. *J. Biomol. NMR* **43**, 187–196 (2009).
29. A. Piai, *et al.*, CON-CON assignment strategy for highly flexible intrinsically disordered proteins. *J. Biomol. NMR* **60**, 209–218 (2014).
30. S. Chhabra, *et al.*, ^{15}N detection harnesses the slow relaxation property of nitrogen: Delivering enhanced resolution for intrinsically disordered proteins. *Proc. Natl. Acad. Sci. U. S. A.* **115**, E1710–E1719 (2018).
31. T. J. Nott, *et al.*, Phase Transition of a Disordered Nuage Protein Generates Environmentally Responsive Membraneless Organelles. *Mol. Cell* **57**, 936–947 (2015).
32. J. Wang, *et al.*, A Molecular Grammar Governing the Driving Forces for Phase Separation of Prion-like RNA Binding Proteins. *Cell* **174**, 688-699.e16 (2018).
33. Y. Lin, S. L. Currie, M. K. Rosen, Intrinsically disordered sequences enable modulation of protein phase separation through distributed tyrosine motifs. *J. Biol. Chem.* **292**, 19110–19120 (2017).
34. B. Tsang, *et al.*, Phosphoregulated FMRP phase separation models activity-dependent translation through bidirectional control of mRNA granule formation. *Proc. Natl. Acad. Sci. U. S. A.* **116**, 4218–4227 (2019).
35. K. Pervushin, R. Riek, G. Wider, K. Wuthrich, K. Wüthrich, Attenuated T_2 relaxation by

mutual cancellation of dipole-dipole coupling and chemical shift anisotropy indicates an avenue to NMR structures of very large biological macromolecules in solution. *Proc. Natl. Acad. Sci. U. S. A.* **94**, 12366–12371 (1997).
36. N. A. Farrow, O. Zhang, A. Szabo, D. A. Torchia, L. E. Kay, Spectral density function mapping using ^{15}N relaxation data exclusively. *J. Biomol. NMR* **6**, 153–162 (1995).
37. G. Cornilescu, A. Bax, Measurement of proton, nitrogen, and carbonyl chemical shielding anisotropies in a protein dissolved in a dilute liquid crystalline phase. *J. Am. Chem. Soc.* **122**, 10143–10154 (2000).
38. H. Geen, R. Freeman, Band-selective radiofrequency pulses. *J. Magn. Reson.* **93**, 93–141 (1991).
39. W. Massefski, A. G. Redfield, Elimination of multiple-step spin diffusion effects in two-dimensional NOE spectroscopy of nucleic acids. *J. Magn. Reson.* **78**, 150–155 (1988).
40. C. Zwahlen, S. J. F. Vincent, L. Di Bari, M. H. Levitt, G. Bodenhausen, Quenching Spin Diffusion in Selective Measurements of Transient Overhauser Effects in Nuclear Magnetic Resonance. Applications to Oligonucleotides. *J. Am. Chem. Soc.* **116**, 362–368 (1994).
41. G. A. Morris, R. Freeman, Enhancement of Nuclear Magnetic Resonance Signals by Polarization Transfer. *J. Am. Chem. Soc.* **101**, 760–762 (1979).
42. D. Marion, M. Ikura, R. Tschudin, A. Bax, Rapid recording of 2D NMR spectra without phase cycling. Application to the study of hydrogen exchange in proteins. *J. Magn. Reson.* **85**, 393–399 (1989).
43. E. Kupče, R. Freeman, Optimized adiabatic pulses for wideband spin inversion. *J. Magn. Reson. - Ser. A* **118**, 299–303 (1996).
44. A. S. Maltsev, J. Ying, A. Bax, Deuterium isotope shifts for backbone ^{1}H, ^{15}N and ^{13}C nuclei in intrinsically disordered protein α-synuclein. *J. Biomol. NMR* **54**, 181–191 (2012).
45. G. Lipari, A. Szabo, Model-Free Approach to the Interpretation of Nuclear Magnetic Resonance Relaxation in Macromolecules. 2. Analysis of Experimental Results. *J. Am. Chem. Soc.* **104**, 4559–4570 (1982).